Self-consistent particle tracking in a simulation of the entropy mode in a Z pinch

K. Gustafson*, I. Broemstrup*, D. del-Castillo-Negrete†, W. Dorland* and M. Barnes*

*Department of Physics, CSCAMM, University of Maryland, College Park 20742
†Oak Ridge National Laboratory, Oak Ridge, TN

Abstract.
A single particle tracking technique for studying nondiffusive transport is implemented in a new particle-in-cell gyrokinetic simulation of the entropy mode in a Z pinch geometry. Radial transport is characterized in terms of the time dependence of the variance of displacements. The vertical zonal flow dynamics of the nonlinear phase of the instability seem to cause subdiffusive transport for ions during the simulation lengths used here. Electrons follow subdiffusive transport, except for later times in the case of the largest gradient, where the transport becomes superdiffusive. The probability distribution of displacements shows a positive skew and long tails relative to the Gaussian distribution for both ions and electrons.

Keywords: Gyrokinetics, microturbulence, Z pinch, entropy mode, nondiffusive transport
PACS: 02.70.Ns, 05.40.Fb, 52.25.Dg, 52.25.Fi, 52.30.Gz, 52.35.Qz, 52.55.Tn

INTRODUCTION

The transport of particles and heat in a turbulent plasma is an area of research with relevance to fusion energy and astrophysical topics. It has been proposed [1, 2, 3, 4] that the nature of the transport is more complex than allowed by a simple Brownian random walk. In particular, it may be necessary to relax the Markovian and Fickian assumptions of locality in time and space to explain the nondiffusive transport of particles inferred in some magnetic fusion devices. Here, we examine the self consistent transport of particles driven by the gyrokinetic entropy mode in a Z pinch [5, 6] as an example of a simplified geometry with curvature and $\nabla\mathbf{B}$ drifts without the added complexity of trapped particles. We look at equal temperature kinetic electrons and ions in the recently developed gyrokinetic δf particle-in-cell code, GSP [7]. A density gradient is used to drive the entropy mode, which displays a fast linear growth phase with streamers in the radial direction followed by a nonlinear zonal flow state with radial transport inhibited. The metric used here for nondiffusive transport is the value of γ for the scaling of the variance of particle displacements in the radial direction, $\sigma_r^2(t) \sim t^\gamma$. The value of γ is related to the parameters of certain models for nondiffusive transport [8, 3].

Z PINCH ENTROPY MODE

The Z pinch, in which a straight vertical current creates a cylindrically symmetric magnetic field, is a useful intermediate step between slab and tokamak geometry. It

CP1069, *Theory of Fusion Plasmas, Joint Varenna-Lausanne International Workshop*
edited by X. Garbet, O. Sauter, and E. Sindoni

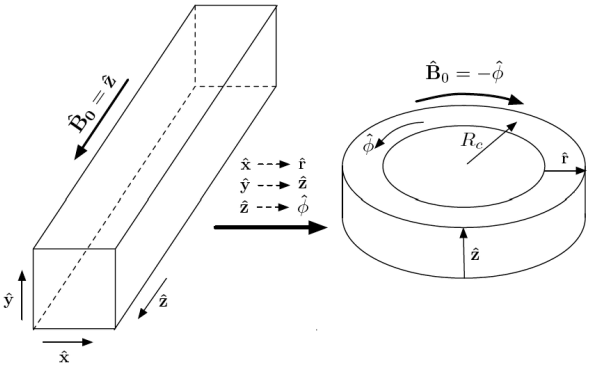

FIGURE 1. Geometry for the Z pinch is a mapping of the (x,y,z) code coordinates to the (r,z,ϕ) coordinates of the Z pinch. The current is in the $\hat{z}$ direction, and the **B** field in purely in the $-\hat{\phi}$ direction.

requires less computational expense because of periodicity in the field direction and, thus, elimination of one spatial dimension. At the same time, the Z pinch includes both the $\nabla\mathbf{B}$ and curvature drifts that produce important instabilities in a tokamak. As shown in Fig. 1, the Z pinch is essentially a cylinder wrapped around so that the **B** field lines are periodic. The static magnetic field is in the toroidal direction, $\hat{\mathbf{B}}_0 = -\hat{\phi}$, with a radial dependence $B \sim 1/r$. A combination of the $\nabla\mathbf{B}$ and curvature drifts gives a drift that is always perpendicular to both the $\hat{r}$ and $\hat{\phi}$ directions and depends on the sign of the charged particle. The $\mathbf{E} \times \mathbf{B}$ drift, on the other hand, is generally in both the $\hat{r}$ and $\hat{z}$ directions.

The entropy mode in the Z pinch has been studied by Ricci, *et al* [6, 9] using gyrokinetic theory and nonlinear calculations with the continuum gyrokinetic code GS2 [10]. This mode exists at weaker pressure gradients than the ideal magnetohydrodynamic interchange mode, and can have growth rates comparable to the ideal mode when the density gradient scale length, $L_n = -n'/n$ is in the proper range ($2/7 < L_n/R_c < \pi/2$, where R_c is the radius of curvature). It was shown that the entropy mode creates radial $\mathbf{E} \times \mathbf{B}$ flows in the linear phase, which break up into zonal flows in the $\hat{z}$ direction during the nonlinear phase because of a Kelvin-Helmholtz instability (KHI).

CODE METHODOLOGY

Particle-in-cell (PIC) methods for numerical solution of the gyrokinetic-Poisson system are in wide use [11, 12]. Several groups have developed sophisticated PIC codes with a range of capabilities, some with the evolution of the full distribution function (full $F = F_0 + \delta f$) and some that evolve only the difference (δf [13]) between a Maxwellian background distribution (F_0). We use the recently developed and benchmarked δf gyrokinetic PIC code, GSP [7]. GSP employs the flux tube approximation and computes

the nonlinear evolution of particle weights, $w_i \equiv \frac{\langle \delta f \rangle_R}{F_0}|_{R_i, v_{\perp i}, v_{\parallel i}}$, using the method of characteristics. Here, $\langle \rangle_R$ is the gyro-average at fixed gyro-center position R. Normalization of the perpendicular coordinate is given by $1/\rho_i$, the parallel coordinate by $1/a$, ϕ by $qa/T_i\rho_i$ and time by $v_{T,i}/a$. Here, ρ_i is the singly-charged ion Larmor radius, $v_{T,i}$ is the ion thermal velocity, q is the charge on the ions and electrons and T_i is the ion temperature. Notably, in gyrokinetics, parallel (to $\hat{b}$) wavelengths are $\mathcal{O}(\varepsilon^{-1})$ larger than perpendicular wavelengths. The order parameter for the gyrokinetic expansion is $\varepsilon \equiv \rho_i/a$ [14], where a is a typical macroscopic length scale. The gyrokinetic equation is taken to $\mathcal{O}(\varepsilon)$ in this work.

GSP has been benchmarked against GS2 and has been shown to have good parallelization for both strong and weak scaling. Two important advances in GSP, which distinguish it from other δf PIC codes, are the implementation of a pitch-angle scattering collision operator and a spectral-space evaluation of the gyro-averages. Utilization of the collision operator is not within the scope of this exploratory study. However, explicit $J_0(k_\perp v_\perp/\Omega)$ evaluation for a more efficient and exact gyro-average is of critical importance for the entropy mode. Many PIC codes use a discrete ring average, with four points to represent the ring, which is only accurate for values of $k_\perp \rho \leq 1$. This is insufficient for the entropy mode in a Z pinch (*c.f.* [15]), for which a significant portion of the turbulent energy is contained in short-wavelength structures.

NONDIFFUSIVE TRANSPORT INDICATIONS

For the results presented here, GSP is run with 20 million particles, which is equivalent to 1220 particles per (r,z,ϕ) grid point for a $128 \times 128 \times 1$ run. Assuming a 16x16 resolution in velocity space, this is 4 particles per phase space cell. The box dimensions are $L_r = L_z = 125.66, L_\phi = 6.28$ and the timestep $\delta t = 0.05$ for the second-order predictor-corrector method used for solving the ODEs from the method of characteristics. Two kinetic species are used: electrons and singly-charged ions with equal temperature, $T_i = T_e$ and mass ratio $m_e/m_i = 5.4 * 10^{-4}$. Since we are interested in following the trajectories of unique particles, it is necessary to track their positions after they leave the box. This is achieved by recording particle positions at a specified time interval without taking the modulus of the position with the box size. This allows particles to travel further than one box length but retains the periodicity of ϕ. We also output the particle weights after each time interval and multiply the weight by the position to get the density of particles at that position. A more thorough discussion of the physical meaning of the displacement of a simulation particle with a time-varying weight will be presented elsewhere.

Nondiffusive transport in the radial direction is characterized the mean $M(t) = \langle \delta r(t) * w(t) \rangle$ and variance $\sigma_r^2(t) = \left\langle (\delta r(t) * w(t) - \langle \delta r(t) * w(t) \rangle)^2 \right\rangle$ of particle displacements $\delta r(t) = r(t) - r(0)$ multiplied by the particle weights, $w(t)$. For diffusive transport, the distribution of step sizes for the random walk is given by a Gaussian distribution and the waiting times between steps are given by a Poisson distribution. This leads to a linear scaling in the variance and the mean, such that $M(t) \sim t$ and $\sigma^2 \sim t$. If transport is nondiffusive, the distributions of step sizes and waiting times are possibly power laws. The scaling in the variance for power law distributions would therefore be $\sigma^2(t) \sim t^\gamma$, where $\gamma < 1$ indicates subdiffusive transport and $\gamma > 1$ indicates superdiffu-

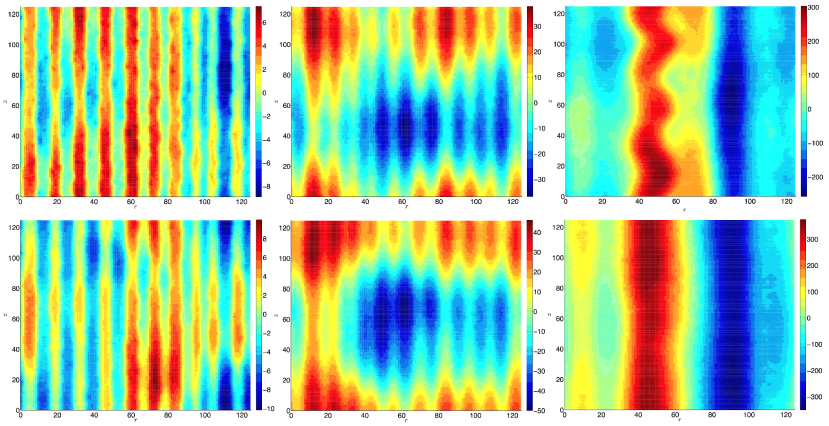

FIGURE 2. (Color online) Electrostatic potential, ϕ, during the nonlinear phase at time points $t = 150$ and $t = 250$. The vertical zonal flow is apparent, but the $k_z \sim 2\pi$ structure seems to allow some radial transport. From left the right, as the gradient increases from $L_n/R_c = \{1.0, 0.75, 0.5\}$, the wavenumber for the zonal flow decreases and the amplitude of the field becomes stronger.

sive transport.

The parameter we are varying in this study is the scale length of the density gradient, L_n, such that a larger scale length gives a weaker gradient. Figure 2 shows the electrostatic field, ϕ, for three different values of L_n/R_c: 1.0, 0.75 and 0.5, at two time points in the nonlinear phase, after the KHI has created the vertical zonal flows. The wave number of the zonal flow is always $k_r\rho_i \sim 1$, but it decreases as L_n decreases. This is consistent with the result in Fig. 4 of [9]. Also consistent with linear gyrokinetic theory is the relative magnitude of ϕ at a given time point, which shows that the growth rate of the entropy mode increases with the strength of the gradient. It seems that some structure appears in the k_z direction at $L_n/R_c = 0.75$. This may have an effect on the radial transport since it opens gaps in the zonal flows.

Direct observation of the full particle distribution function (PDF) shows that the spreading of particles is skewed in the $+\hat{r}$ direction. The tails of the PDF for the largest gradient are extended beyond the Gaussian shape of diffusive transport, as shown in Fig. 3. The second moment of the PDF indicates that the spreading of displacements are nondiffusive, as shown in Fig. 4. During the linear phase of the entropy mode, the variance of displacements grows extremely quickly because of the radial streamers. As the KHI appears in the nonlinear phase, the zonal flows slow the spreading for both electrons and ions. The ion spreading is subdiffusive for each value of the gradient studied, with two distinct values of γ as listed in Table 1 and shown in Fig. 4.

CONCLUSIONS

Grid resolution for r-z space must be carefully checked for GSP simulations. Higher spatial resolution will significantly increase the number of particles required in the

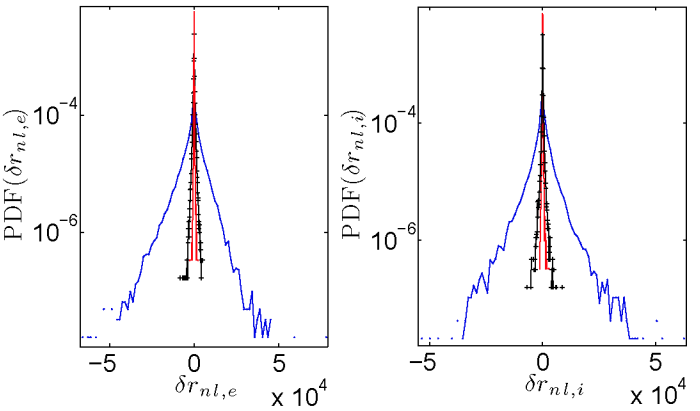

FIGURE 3. (Color online) Probability distribution of radial displacements for 40 000 ions and 40 000 electrons in the Z pinch for the nonlinear phase of the entropy mode. The δf particle positions are multiplied by the weights. From outside to inside, the strength of the gradient decreases, from $L_n/R_c = \{0.5, 0.75, 1.0\}$. Ions are on the right panel, electrons are on the left. Displacements are measured relative to the particle positions at the end of the linear growth phase of the instability. A positive skew is seen for all values of the density gradient, and long tails are also apparent.

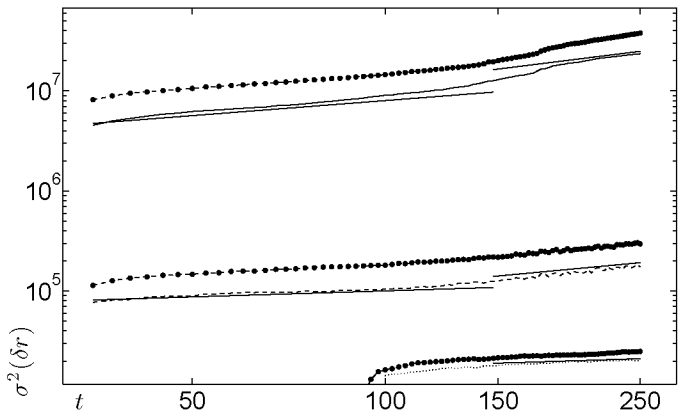

FIGURE 4. Variance of displacements in the radial direction during the nonlinear phase of the entropy mode instability. The δf particle positions are multiplied by the weights. Two distinct regimes in time are noticed, both with nondiffusive values of γ. The strength of the gradient decreases from top to bottom, from $L_n/R_c = \{0.5, 0.75, 1.0\}$. The electrons are shown by traces with markers and are always shifted up from the ions. Straight lines indicate the values of γ listed in Table 1.

simulation. If the weights are observed to be growing too fast (because of large fluxes), the pitch-angle scattering collision operator can be used to control that growth without being forced into using very large numbers of particles.

TABLE 1. Nondiffusive transport exponents in the nonlinear phase for electrons and ions separated into two regimes in time.

L_n/R_c	$\gamma_{1,i}$	$\gamma_{2,i}$	$\gamma_{1,e}$	$\gamma_{2,e}$
1.0	0.5	0.8	0.45	1.2
0.75	0.2	0.6	0.2	0.55
0.5	0.2	0.2	0.25	0.25

Fast growth of the radial variance in the linear phase comes from the presence of radially directed velocity streamers, which give way to vertical zonal flows and subdiffusive radial spreading. The nonlinear phase shows nondiffusive transport, with two distinct values of γ at different times for stronger gradients, and only one value for the weakest gradient. The ions show strictly subdiffusive spreading. The electrons in the strongest gradient experience a transition from subdiffusive to superdiffusive spreading. Future work will show how collisions affect the nondiffusive transport metrics, since collisions tend to decrease the coherence of zonal flows [9].

ACKNOWLEDGMENTS

This work is supported by the Fannie and John Hertz Foundation and the U.S. Department of Energy through the Center for Multiscale Plasma Dynamics. D. del-Castillo-Negrete acknowledges support from the Oak Ridge National Laboratory, managed by UT-Battelle, LLC, for the U.S. Department of Energy under contract DE-AC05-00OR22725

REFERENCES

1. D. del Castillo Negrete, *Phys. Plasmas* **7**, 1702 (2000).
2. S. V. Annibaldi, G. Manfredi, and R. O. Dendy, *Phys. Plasmas* **9**, 791 (2002).
3. R. Sanchez, B. van Milligen, and B. Carreras, *Physics of Plasmas* **12**, 056105 (2005).
4. D. del Castillo Negrete, *Phys. Plasmas* **13**, 082308 (2006).
5. A. N. Simakov, P. J. Catto, and R. Hastie, *Physics of Plasmas* **8**, 4414 (2001).
6. P. Ricci, B. N. Rogers, W. Dorland, and M. Barnes, *Physics of Plasmas* **13**, 062102 (2006).
7. I. Broemstrup, *Advanced Lagrangian Simulation Algorithms for Magnetized Plasma Turbulence*, Ph.D. thesis, University of Maryland, College Park (2008).
8. D. del Castillo Negrete, *Phys. Plasmas* **11**, 3854 (2004).
9. P. Ricci, B. N. Rogers, and W. Dorland, *Physical Review Letters* **97**, 245001 (2006).
10. M. Kotschenreuther, G. Rewoldt, and W. M. Tang, *Computational Physics Communications* **88**, 128 (1995).
11. W. W. Lee, *Physics of Fluids* **26**, 556 (1983).
12. S. Brunner, E. Valeo, and J. Krommes, *Physics of Plasmas* **6**, 4504 (1999).
13. A. M. Dimits, and W. W. Lee, *Journal of Computational Physics* **107**, 309 (1993).
14. E. A. Frieman, and L. Chen, *Physical Review Letters* **97**, 245001 (2006).
15. J. Kesner, *Physics of Plasmas* **7**, 3837 (2000).